Modeling Adsorbate-Induced Property Changes of Carbon Nanotubes

Lynn Groß,[a] Marc Philipp Bahlke,[a] Torben Steenbock,[a] Christian Klinke,[b] and Carmen Herrmann *[a]

Because of their potential for chemical functionalization, carbon nanotubes (CNTs) are promising candidates for the development of devices such as nanoscale sensors or transistors with novel gating mechanisms. However, the mechanisms underlying the property changes due to functionalization of CNTs still remain subject to debate. Our goal is to reliably model one possible mechanism for such chemical gating: adsorption directly on the nanotubes. Within a Kohn–Sham density functional theory framework, such systems would ideally be described using periodic boundary conditions. Truncating the tube and saturating the edges in practice often offers a broader selection of approximate exchange–correlation functionals and analysis methods. By comparing the two approaches systematically for NH_3 and NO_2 adsorbates on semiconducting and metallic CNTs, we find that while structural properties are less sensitive to the details of the model, local properties of the adsorbate may be as sensitive to truncation as they are to the choice of exchange–correlation functional, and are similarly challenging to compute as adsorption energies. This suggests that these adsorbate effects are nonlocal. © 2017 Wiley Periodicals, Inc.

DOI: 10.1002/jcc.24760

Introduction

The response of carbon nanotubes (CNTs) to adsorbed molecules has been the subject of intensive research in the past few years. They are important as building blocks for a variety of potential applications in nanotechnology, such as highly sensitive low-power chemical sensors,[1–5] which may be used, for example, as wake-up detectors for power-consuming accurate sensors for air quality monitoring.[6] In particular, noncovalent adsorption can modify the CNTs' static electronic and electron transport properties, while the atomic structure of the CNTs is not significantly perturbed compared with covalent adsorption.[7–9] As the first reports on detecting gaseous molecules with individual single-walled CNTs were published in 2000,[10,11] the effect of adsorption on the conductivity of CNTs is being controversially discussed in the literature.[12–21] There are several aspects that have to be taken into account. In transistors, the nanotube is contacted by (typically) metallic electrodes acting as source and drain.[2] Thus, gas adsorption may occur on the metal surface, on the nanotube surface, or at the interface between the tube and the electrode.[21] Given the sometimes contradictory statements in the literature and the complexity of these systems, theoretical studies are required for elucidating the mechanism underlying sensing behavior and chemical gating. They have mainly focused on understanding the adsorbate–nanotube interactions within the channel region, proposing different mechanisms responsible for shifts in the transistor characteristics, such as dissociative adsorption of NO_2,[15,22–24] increased gas concentration,[18] charge transfer (NH_3 molecules acting as donors and NO_2 molecules acting as acceptors),[25–30] and changes in the adsorbates' dipole moment.[18] Recent theoretical investigations suggested that NH_3 and NO_2 physisorb on the CNT and chemisorb at the contact region, while the latter is suggested to be the dominant mechanism affecting the conductance.[21] Note, however, that these results are contingent on the detailed atomistic interface structure, which was assumed to feature covalent carbon–gold bonds between the CNT and a gold surface.

Owing to its computational efficiency, Kohn–Sham density functional theory (KS-DFT)[31] is the only first-principles method to date capable of dealing with structures that allow for a realistic modeling of CNT–adsorbate interactions. While exact in principle, in practice the exchange–correlation functional has to be described by one of many established approximations. Due to their quasi-one-dimensional nature, CNTs are usually modeled imposing periodic boundary (PB) conditions. This may require a large unit cell[32–34] to account for the extended nature and complexity of chemically gated single-walled CNT transistors. An even more crucial point is the (in practice) often limited choice of pseudopotentials in plane-wave codes (and thus the limited choice of exchange–correlation functionals). Also, many periodic-boundary electronic-structure codes cannot provide an all-electron description. In contrast, an approach using truncated CNTs saturated with hydrogen atoms can often take advantage of a larger pool of

[a] L. Groß, M. P. Bahlke, T. Steenbock, C. Herrmann
Department of Chemistry, Institute for Inorganic and Applied Chemistry, University of Hamburg, Martin-Luther-King-Platz 6, Hamburg 20146, Germany
E-mail: carmen.herrmann@chemie.uni-hamburg.de
[b] C. Klinke
Department of Chemistry, Institute for Physical Chemistry, University of Hamburg, Grindelallee 117, Hamburg, 20146, Germany
Contract grant sponsors: German Research Foundation DFG project KL 1453/9-1 (to C.K.) and DFG project B17 in SFB 668 (to C.H, T.S., and L.G.)

exchange–correlation functionals, which is in some cases essential even for an accurate qualitative description, enables estimating the DFT error,[35] and allows for easy interfacing with various quantum chemical analysis tools. However, the most serious error source of truncation is the choice of a too small CNT size (involving capping atoms such as hydrogen, where necessary), which may lead to inaccurate structural properties (e.g., a preferred adsorption at the edge). Moreover, truncating the nanotube produces discrete single-particle levels (molecular orbitals) rather than bands, and the number of these levels decreases with the decreasing lengths of the tubes, thus leading to an electronic structure less and less suitable for approximation of the CNT band structure. Thus, assessing whether a truncated approach can reproduce the results obtained under PB conditions provides an essential step toward a reliable theoretical description of adsorbate–CNT interactions. This also answers a more fundamental question, namely how "local" the binding between CNT and adsorbate is, and to what extent the CNT band structure is crucial for this binding.

In this work, we systematically compare structural and local properties using two different commonly used density functional theory approaches, (1) a truncated model (based on localized, atom-centered single-particle basis functions) and (2) a PB approach using a plane-wave basis.* Both have their shortcomings (which were briefly mentioned and will be discussed in more detail below), but as calculations avoiding these limitations (i.e., using very large unit cells or long truncated tubes, using all-electron basis sets close to the basis set limit with sharp convergence criteria) are often not feasible in practice, for example when scanning adsorption positions for large molecular adsorbates, it is important to identify how sensitive different physical quantities are to the choices made in terms of computational model, and to what extent they are robust enough to be evaluated from a less-than-perfect computation. Our goal is to provide guidelines for suitable molecular adsorbates on CNTs. As well-established adsorption structures exist for metallic and semi-conducting CNTs functionalized with NH_3 and NO_2, respectively, these were used as benchmark systems. Moreover, we focus on NH_3 as an example of a "simple" physisorbed molecule and on NO_2 providing a more challenging test case due to its open-shell nature and its potential for charge transfer and chemisorption.

Computational Methodology

All calculations were carried out using KS-DFT.

Methods and model systems

Spin-restricted closed-shell calculations were performed for NH_3 and pure CNT systems, and spin-unrestricted ones for NO_2 systems (which formally contain one unpaired electron). As several reports on the adsorption mechanism of NH_3 and NO_2 on single-walled CNTs showed that the binding energy is quite insensitive to the adsorption position[15,26,27] (within a given method), only one orientation of the attached molecule was studied here. At the beginning of each structure relaxation, the respective adsorbate is placed in an upright position on top of a carbon atom. The NO_2 molecule is arranged perpendicular to the single-walled CNT surface (with the oxygen atoms pointing away from it). The NH_3 molecule is adsorbed such that the hydrogen atoms are pointing toward the nanotube. On optimization, the adsorbates may tilt or move to different adsorption positions. Optimized molecular structures under PB conditions were obtained with the quantum chemical program package QUANTUM ESPRESSO 5.0,[39] which uses plane-wave single-particle basis functions to account for the valence electrons and pseudopotentials for treating nuclei plus core electrons. Projector-augmented plane-wave pseudopotentials generated with the generalized gradient approximation PBE functional (PAW-PBE)[40] were used. A kinetic energy cutoff of 47 (264) Ry for the wavefunction (charge density) is used, and tested to give converged results for the total energy. The unit cells consist of either a semi-conducting (8,0) $25\times25\times8.87$ Å^3 (64 atoms) or a metallic (5,5) $25\times25\times6.89$ Å^3 (60 atoms) CNT using a $1\times1\times16$ Monkhorst-Pack-Grid with a Marzari-Vanderbilt smearing of 0.02 Ry to sample the Brillouin zone, unless otherwise stated (see the input files in Section 9 of the Supporting Information). The size of one unit cell is considered to be sufficiently large, so that intermolecular interactions are assumed to be negligible (this assumption may be only partially fulfilled, see the discussion below). For the isolated molecules a $50\times50\times50$ Å^3 unit cell was used using the Γ point to sample the Brillouin zone. As dispersion interaction is important for the adsorption of molecules on surfaces or nanotubes, we performed all calculations without and with Grimme's semi-empirical D2 correction scheme.[41] If not noted otherwise, the QUANTUM ESPRESSO 5.0 default convergence criteria were used. For comparison, we carried out additional optimizations with PBE-D2 using the same sharp convergence criteria as used in the TURBOMOLE calculations on truncated structures as detailed below. The truncated approach is considered next. All truncated electronic structure calculations were performed using the quantum chemical program package TURBOMOLE 6.5[42] with the PBE functional[43–45] and Ahlrichs' split-valence triple-zeta basis set with polarization functions on all atoms (def-TZVP).[46] Additional molecular structure optimizations were performed using the pure approximate exchange–correlation functional BP86[47,48] and the hybrid functional B3LYP,[49,50] with 20% of exact exchange admixture. Dispersion interactions were taken into account via Grimme's semi-empirical D2[41] scheme and Grimme's more recent D3 method[51] with Becke–Johnson (BJ) damping.[52] The convergence criterion in the self-consistent field algorithm was a change of energy below 10^{-7} Hartree. The convergence criterion in the structure optimization was a gradient of 10^{-4} Hartree/Bohr. We used the resolution-of-the-identity approximation as implemented in TURBOMOLE 6.5 in combination with the two pure functionals. A semi-conducting (8,0) and a metallic (5,5) truncated CNT of two different lengths (short: 8 Å; long: 19 Å) were used as

*Of course, there are also some electronic-structure codes which combine periodic boundary conditions with localized basis functions such as CP2K,[36] ADF,[37] and GAUSSIAN.[38]

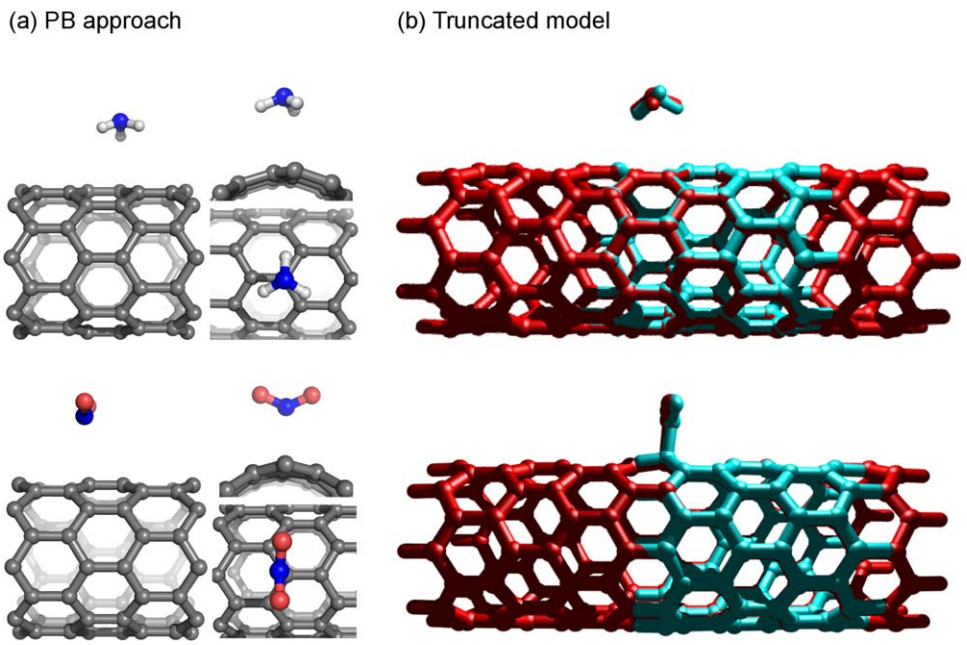

Figure 1. PBE-D2 optimized structures of NH_3 (top) and NO_2 (bottom) on a semi-conducting (8,0) CNT using a PB model and a truncated approach with two different tube lengths (blue: 8 Å; red: 19 Å). [Color figure can be viewed at wileyonlinelibrary.com]

model systems (see Supporting Information for Cartesian coordinates of these and all other structures). To reduce boundary effects, atoms at the open ends of the tube have been saturated by hydrogen atoms. The adsorption energy (E_a) is defined as the difference between the energy of the total molecule–CNT system ($E_{mol-CNT}$) and the summed up energy of the pristine CNT (E_{CNT}) and the isolated gas molecule (E_{mol}),

$$E_a = E_{mol-CNT} - (E_{CNT} + E_{mol}). \quad (1)$$

The initial structures of the CNTs were generated with AVOGADRO.[53] Given that it is not relevant for plane-wave calculations, and given the relatively large size of the used atom-centered basis set, the basis superposition error was assumed to be negligible. Molecular structures were mainly visualized with PYMOL[54] and MOLDEN.[55]

For single-point electronic structure calculations on top of structures optimized under PB conditions, the PBE-D2 optimized structures obtained by the PB approach were saturated with hydrogen atoms at the open ends of the tube. While all atoms were held fixed, the hydrogen atoms of the tube were optimized with a truncated approach using PBE-D2/def-TZVP. Then, single-point electronic structure calculations were performed using different exchange–correlation functionals. Also here, we additionally studied longer tubes for comparison, which, in contrast to the optimized structures, were constructed by saturating three consecutive unit cells from the PBE-D2 optimized structures obtained by the PB approach with hydrogen and relaxing the hydrogen atoms, as above. This ensures that the comparison with the PB structures is not affected by any periodic image effects[32–34] which may be present, as both the (long) truncated and the PB calculation will be affected by it equally.

Cutting the nanotubes as described above and as shown in Figure 1 may result in electronic structures with an open-shell ground state. This may be prevented by cutting the tubes in a less "straight" fashion, such that Clar sextet theory is taken into account.[56] In our study, this distinction affects the semi-conducting (8,0) CNTs, for which we are thus comparing our data to both optimized structures and single-point calculations on top of the PBE-D2 optimized structures obtained by the PB approach, which were truncated according to Clar's rules (see Figure S9 in the Supporting Information for structures).

Local properties within the theory of atoms-in-molecules

We define the amount of charge transfer from the adsorbates to the nanotube as the sum of Bader charges of atoms *i* in the adsorbate molecule. As well as other density-based partitioning schemes such as the Hirshfeld approach,[57] Bader's atoms-in-molecules (AIM) analysis[58–61] it is not very sensitive to the basis set used in the electronic structure calculation.[62,63] This is a clear advantage over approaches that are based on atom-centered one-particle basis functions, such as the Mulliken[64] and the Löwdin[65] population analysis. Within the theory of AIM, the local dipole moment of an atom *i* can be defined as the sum of a polarization $\boldsymbol{\mu}_i^p$ and a charge transfer $\boldsymbol{\mu}_i^c$ contribution.[66] While the dipole moment for the total (uncharged) adsorbate–CNT system is independent of the choice of origin, the dipole moment of the adsorbed molecule can be origin-dependent due to the charge transfer from or to the nanotube. To overcome the origin-dependence, we used a modified version of Bader's and Laidig's approach[67,68] to achieve origin-independence of adsorbates' dipole $\boldsymbol{\mu}_{mol}$ by referring to an internal reference point $\boldsymbol{X}^{ref}$ as implemented in the GENLOCDIP tool,[69,70]

Table 1. Preferred adsorption sites,[a] orientations,[b] distances d (in Å), angles θ (in °), adsorption energies $-\boldsymbol{E}_a$ (in eV), partial charges q (in unit charges), and local dipole moments μ (in Debye) of a NH_3 molecule on a metallic (5,5) and a semi-conducting (8,0) carbon nanotube using a periodic-boundary (PB) code and a truncated approach[c] with two different tube lengths.

			PB (PB sharp conv.)		Truncated short/long (Clar)			
System		Property	PBE	PBE-D2	PBE-D2	PBE-D3(BJ)	BP86-D3(BJ)	B3LYP-D3(BJ)[d]
NH_3	Metallic (5,5) CNT	Position	T(T)	T(T)	H/T	T/T	B/T	T/T
		Orient.	↑(↑)	↑(↑)	↗ / ↑	↗ / ↑	↑/↑	↗ / ↑
		d_{N-H}	1.02(1.02)	1.02(1.02)	1.02/1.02	1.02/1.02	1.02/1.02	1.01/1.01
		d_{N-C}	3.90(4.06)	3.38(3.44)	3.33/3.41	3.53/3.49	3.40/3.41	3.52/3.52
		θ_{H-N-H}	106(106)	106(106)	106/106	106/106	106/106	107/107
		$-E_a$	0.00	0.08	0.18/0.13	0.15/0.13	0.15/0.14	0.13/0.12
		q_{NH_3}	0.00	0.00	0.00/0.00	0.00/0.00	0.00/0.00	0.00/0.00
		μ_{NH_3}	1.55	1.69	1.92/1.85	1.92/1.85	1.92/1.85	1.99/1.92
	Semi-cond (8,0) CNT	Position	T(T)	T(T)	H/H(H)	H/H	H/T	H/T
		Orient.	↑(↑)	↑(↑)	↗ / ↑(↑-↗)	↗ / ↑	↗ / ↑	↗ / ↑
		d_{N-H}	1.02(1.02)	1.02(1.02)	1.02/1.02(1.02)	1.02/1.02	1.02/1.02	1.02/1.01
		d_{N-C}	3.92(4.06)	3.23(3.47)	3.38/2.97(3.45)	3.50/3.11	3.45/3.34	3.53/3.41
		θ_{H-N-H}	106	106	106/106(106)	106/106	106/106	107/107
		$-E_a$	0.00	0.07	0.17/0.16(0.17)	0.16/0.16	0.33/0.13	0.30/0.22
		170027	0.00	0.00	0.02/0.02 (0.02)	0.02/0.02 (0.02)	0.02/0.02 (0.02)	0.01/– (–)
		μ_{NH_3}	1.54	1.69	1.76/1.70 (1.72)	1.76/1.70 (1.72)	1.75/1.70 (1.71)	1.85/– (–)

[a] T: top of a carbon atom, H: center of a carbon hexagon, and B: center of C—C bond;. [b] ↑: upright and ↗: tilted;. [c] For the truncated tubes, partial charges q and local dipole moments μ correspond to single-point calculations on top of PBE-D2-optimized structures under PB conditions;. [d] For NH_3–(8,0) CNT, q and $\boldsymbol{\mu}$ of the B3LYP-D3 calculation are not shown due to convergence problems. A "–" entry denotes that a calculation could not be converged.

$$\boldsymbol{\mu}_{mol} = \sum_{i \in mol} \left[\boldsymbol{\mu}_i^p + \boldsymbol{\mu}_i^c\right] = \sum_{i \in mol} \boldsymbol{\mu}_i^p + \sum_{i \in mol} \left[\boldsymbol{X}_i - \boldsymbol{X}^{ref}\right] q_i. \quad (2)$$

with the atomic polarization $\boldsymbol{\mu}_i^p = -\int_A \boldsymbol{r}_A \rho(\boldsymbol{r}) d\boldsymbol{r}$, the nuclear coordinate $\boldsymbol{X}_i$ and the net charge q_i of an atom i in the gas molecule. Local charges and atomic polarizations were obtained using the grid-based Bader tool written by the Henkelman group[71–73] which is well suited for large solid-state physical systems due to its computational efficiency. Each volume element of the three-dimensional grid is 0.10 units wide. Molecular structures, reference points, and dipole moments are visualized with POVray[74] and a local postprocessing tool. The dipole moment is indicated as a red arrow which points to the positive part ($\delta+$). The local dipole vector of a fragment is visualized such that 1 Debye (D) corresponds to 2 Å, and that the middle of the vector is located at the center of mass of the fragment. The internal reference point between the molecule and the nanotube (marked as a green dot) is defined such that the grid point of the Bader volume of the fragment closest to an atom of the residual group is used to drop a perpendicular from this point to the straight line connecting the molecule and the tube. The system is partitioned into two subsystems as illustrated in Figure S10 in the Supporting Information.

Results and Discussion

In the following, we discuss structures, adsorption energies, local charges and dipole moments for NO_2 and NH_3 molecules adsorbed on semi-conducting (8,0) and on metallic (5,5) single-walled CNTs using PB conditions on the one hand, and on the other hand truncated nanotubes of two different lengths. We additionally evaluate the effect of tighter convergence criteria on the PB optimized structures, and of cutting tubes according to Clar sextet theory rather than "straight." The results for NH_3 and NO_2 adsorption on metallic (5,5) and semi-conducting (8,0) CNT are given in Tables 1 and 2, respectively.

Adsorption energies and structures

Both NO_2 and NH_3 molecules adsorb with the nitrogen on top of a carbon atom in an upright orientation using the PB approach, regardless of whether including (see Fig. 1a and Figures S7 and S8 in the Supporting Information) or not including dispersion corrections.[†]

For adsorbed NH_3, the adsorption energy calculated including dispersion correction is very small, independent of the electronic nature of the nanotube (metallic:–0.08 eV; semi-conducting: −0.07 eV). If Grimme's D2 dispersion correction is not included in the calculations, there is no binding of the NH_3 to the nanotube at all. This is in line with previous computational findings in the literature,[26,27] but may be affected by unwanted interactions between adjacent unit cells. For NO_2 adsorption, the adsorption energy calculated including dispersion correction for NO_2 on a metallic (5,5) CNT is twice as high (−0.53 eV) as for their semi-conducting counterpart (−0.17 eV), which has also been found in Ref. [75]. The interaction between the NO_2 molecule and the CNT is weaker if dispersion correction is not included in the calculations. Adsorption distances (measured as the shortest d(C–N)) are roughly the same when comparing semi-conducting with metallic CNTs.

[†]If not explicitly mentioned otherwise, the following refers to calculations including dispersion correction.

Table 2. Preferred adsorption sites,[a] orientations,[b] distances d (in Å), angles θ (in °), adsorption energies $-E_a$ (in eV), partial charges q (in unit charges), and local dipole moments μ (in Debye) of a NO_2 molecule on a metallic (5,5) and a semi-conducting (8,0) carbon nanotube using a periodic-boundary (PB) code and a truncated approach[c] with two different tube lengths.

			PB (PB sharp conv.)		Truncated short/long (Clar)			
System		Property	PBE	PBE-D2	PBE-D2	PBE-D3(BJ)	BP86-D3(BJ)	B3LYP-D3(BJ)
NO_2	Metallic (5,5) CNT	Position	T(T)	T(T)	T/T	T/T	T/T	T/B
		Orient.	↑(↑)	↑(↑)	↗ / ↗	↗ / ↗	↗ / ↗	↗ / ↗
		d_{N-O}	1.22(1.22)	1.22(1.22)	1.22/1.22	1.22/1.22	1.22/1.22	1.20/1.20
		d_{N-C}	3.30(3.32)	2.96(2.93)	2.97/2.87	2.99/2.92	2.95/2.84	3.00/3.03
		θ_{O-N-O}	129(130)	129(129)	129/130	129/130	129/130	131/133
		$-E_a$	0.43	0.53	0.25/0.20	0.25/0.20	0.27/0.22	0.18/0.16
		q_{NO_2}	−0.22	−0.22	−0.16/–0.17	−0.16/–0.17	−0.17/–0.18	−0.11/–0.13
		μ_{NO_2}	2.16	2.16	1.70/1.71	1.70/1.71	1.75/1.75	1.36/1.52
	Semi-cond. (8,0) CNT	Position	T(T)	T(–)	T/T(T-B)	T/T	T/T	T/T
		Orient.	↑(↑)	↑(–)	↑/↑(↗)	↑/↑	↑/↑	↑/↑
		d_{N-O}	1.22(1.22)	1.22(–)	1.23/1.22(1.21)	1.23/1.22	1.23/1.22	1.22/1.21
		d_{N-C}	3.44(3.44)	2.95	1.58/1.77(2.84)	1.58/1.75	1.58/1.77	1.58/1.67
		θ_{O-N-O}	131(131)	131	126/128(132)	126/128	126/128	126/127
		$-E_a$	0.08	0.17	2.08/0.74(0.18)	2.07/0.71	2.08/0.77	2.71/1.64
		q_{NO_2}	−0.16	−0.16	−0.16/–0.15 (−0.06)	−0.16/–0.15 (−0.06)	−0.16/–0.15 (−0.07)	−0.08/–0.09 (−0.02)
		μ_{NO_2}	1.63	1.66	1.55/1.44 (0.72)	1.55/1.44 (0.72)	1.56/1.47 (0.77)	1.01/1.06 (0.53)

[a] T: top of a carbon atom, H: center of a carbon hexagon, and B: center of C—C bond;. [b] ↑: upright and ↗: tilted;. [c] For the truncated tubes, partial charges q and local dipole moments μ correspond to single-point calculations on top of PBE-D2-optimized structures under PB conditions. A "–" entry denotes that a calculation could not be converged

For NH_3, the distances are larger by 50−60 pm than for NO_2. Using dispersion corrections shortens the distance by 50−70 pm for NH_3 and by 30−50 pm for NO_2. Other lengths and angles are just as for the isolated molecules when optimized with the same computational settings. When going from the QUANTUM ESPRESSO default convergence criteria to the tighter ones used in the TURBOMOLE calculations, the distance between the NH_3 adsorbate and the CNT decreases by up to 22 pm, which indicates that the potential energy surface is quite flat in the bonding region for this system. In contrast, NO_2 is barely affected in this way, which is in line with its larger adsorption energy. Importantly, all other structural parameters are unaffected by tightening the convergence criteria for both molecules.

The truncated approach is considered next. For short truncated nanotube lengths, we obtain different adsorption sites (at the top of a carbon atom, at the center of a hexagon or at the center of a C—C bond) for NH_3 molecules on a metallic CNT depending on the functional and on the type of dispersion correction used. In all cases, an adsorption structure is obtained which differs substantially from the PB one for the short truncated tube when using the same functional as in the PB case (PBE-D2). Extending the nanotubes' lengths leads to NH_3 adsorption above a carbon atom (T) in an upright orientation on a metallic and semi-conducting tube for most cases which is consistent with the PB results. For NH_3 on a metallic (5,5) tube, the structural parameters of the truncated model are in very good agreement with the PB approach. The exception is the NH_3–(8,0) CNT system using PBE-D2 or PBE-D3: here, the structure optimization leads to hollow-site adsorption. Thus, the PBE-D2 structures from the truncated approach are not generally in agreement with the PBE-D2 PB calculation. All adsorption energies are within the range of −0.12 to −0.33 eV, which is a little larger than the binding energies obtained using the PB model. Cutting the CNT such that Clar sextet theory is obeyed leads to much better agreement with the structural parameters from the PB optimization, in particular the N—C bond distance from the PB optimization using sharp convergence criteria of 3.47 Å is nearly perfectly matched. This is in line with the results by Martínez et al., who found that the finite-size Clar cell models provide a better description for the reactivity of CNTs than the corresponding Kekulé structures.[76] However, the adsorption energy changes only barely. This may be related to differences between the two approaches in terms of pseudopotentials and interactions between periodic images.[32–34] A quite large sensitivity of adsorption energies with respect to computational parameters has frequently been reported in the literature. The local properties obtained from "Clar-cut" single-point calculations on top of PB optimized structures agree well with the full PB approach, which was also the case for the analogous "straight-cut" calculations.

For both truncated metallic tube lengths, NO_2 molecules are adsorbed in top position,‡ however, they are slightly tilted to one side (30°−40°) in contrast with the PB description. The binding energies are calculated to be between −0.16 and −0.27 eV, which is smaller than the energy obtained with the PB approach (−0.53 eV). The optimized structures of NO_2 molecules on semi-conducting CNTs with different tube lengths is shown on the left-hand side of Figure 1. The molecules are adsorbed upright in T position, but in contrast to the proposed physisorption mechanism in the literature and to the

‡Except for NO_2 on a truncated long (5,5) CNT using B3LYP-D3(BJ).

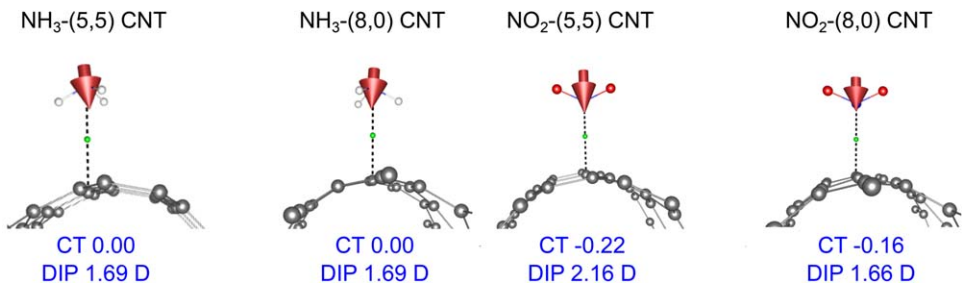

Figure 2. Local dipole moments (in Debye) and charge transfer (in unit charges) of NH_3 (left) and NO_2 (right) molecules adsorbed on a metallic (5,5) and a semi-conducting (8,0) CNT, respectively. PB approach: PBE-D2. [Color figure can be viewed at wileyonlinelibrary.com]

relaxed structures using the PB approach (see right-hand side of Fig. 1), we obtain very short N–C distances for short and longer tube lengths (1.58 Å and 1.77 Å, respectively), and large binding energies in the range of chemisorption ($E_a \leq -0.80$ eV). Truncating the tube according to Clar sextet theory again improves the agreement between PB-optimized and truncated-optimized structures considerably: Physisorption is obtained, as in the PB optimizations, with very good agreement in terms of structural parameters. Interestingly, in contrast to NH_3, the adsorption energies match the ones from the PB calculations, while the local properties differ considerably. Again, apart from the lack of PB conditions, this may be related to the differences in terms of pseudopotentials and interactions between periodic images[32–34] in the two approaches, even though the distance between adsorbates in our periodic structures is reasonable large (the unit cell size of 6.89 to 8.68 Å used in our work leads to intermolecular distances of roughly 5–8 Å).

Changes in local properties due to adsorption

Even if structures are not adequately reproduced by the truncated approach, it would be interesting to know whether this approach can be used for single-point electronic structure calculations on top of structures optimized under PB conditions, as this would still allow studying the dependence of electronic properties on settings such as the exchange–correlation functional, and postprocessing with different analysis methods. Therefore, the quantities most relevant for a qualitative understanding of chemical gating, namely partial charges q and local dipole moments μ of the adsorbates[67–70] are shown in Tables 1 and 2. In Figure 2, the PB charge transfer between adsorbates and nanotubes and the adsorbates' dipole moments[§] obtained from AIM analysis in combination with our generalized local dipole scheme[69,70] are depicted. The partial charges show fairly little charge transfer from the NH_3 to the nanotube, in agreement with the literature.[25–27,81] The local dipole moment of the NH_3 molecule does not change for different tube chiralities (1.69 D) and is a little larger than the dipole moment for an isolated NH_3 molecule (1.48 D, see Table S1 in the Supporting Information). For the NO_2-CNT system, the total charge transfer from the metallic (semi-conducting) tube to the NO_2 molecule (0.16−0.22 unit charges for PB/PBE-D2) indicates that NO_2 acts as an acceptor. The NO_2 molecules' dipole moment increases strongly due to adsorption compared to the dipole moment of an isolated molecule (0.2 D to 0.3 D). The local dipole moment of NO_2 on a metallic CNT is about 0.5 D larger than the one of NO_2 on a semi-conducting CNT (1.66 D).

In accordance with the PB results, the truncated approach also indicates that the charge transfer between NH_3 molecules and nanotubes is negligible. The dipole moment of NH_3 molecules on truncated metallic nanotubes is 1.92 D for a short and 1.85 D for a longer tube length (with PBE-D2), which is too large by 0.15−0.2 D. On semi-conducting tubes, the NH_3 molecules' dipole moments are within the range of 1.70−1.85 D, with the long-tube PBE-D2 results being about 0.10 D larger than the ones obtained with the PB approach. As the deviation between, for example, the truncated PBE and B3LYP results is of similar magnitude, this implies that the PBE-D2 results differ more from the PB/PBE-D2 data than the truncated values among themselves when using different exchange–correlation functionals. The AIM analysis for the truncated tubes shows large charge transfer from the nanotube to the NO_2 molecule (about −0.16 unit charges for PBE-D2) for adsorption on metallic and semi-conducting nanotubes, comparable with the PB approach. Here, the deviations between truncated and PB approach are indeed smaller than between functionals. The dipole moment of NO_2 on truncated (5,5) CNTs scatters between 1.37 D and 1.77 D, depending on the functional and the type of dispersion correction used. The deviations between truncated and PB approach are about as large as between different functionals. On semi-conducting nanotubes, the NO_2 molecules' dipole moment is calculated to be around 1.01−1.55 D, which is a little smaller compared with the PB approach. As mentioned above, cutting the nanotubes according to Clar sextet theory leads to strong deviations in local properties from both the PB approach and the "straight-cut" tubes, in contrast to NH_3.

The fact that a "straight" truncated (and capped) tube built from three repeating unit cells (and thus featuring three adsorbates) gives very good agreement in terms of local properties with the results obtained under PB conditions, while "Clar" truncated structures (which do not take into account interactions between adsorbates in adjacent unit cells) differ. This suggests that these interactions between periodic images play an important role for the electronic (but not structural)

[§]Alternatively, subsystem DFT-based embedding approaches[77–80] may be used to calculate the adsorbates' dipole moments of such adsorbate–CNT systems.

Table 3. Overview of agreement between results for short and long truncated CNTs with reference results obtained under PB conditions.

	NH_3		NO_2	
	Metallic (5,5)	Semicond. (8,0)	Metallic (5,5)	Semicond. (8,0)
Adsorption	Physisorption	Physisorption	Physisorption	Chemisorption
Position	Short: ✗ Long: ✓	✗	✓	✓
Orientation	Short: ✗ Long: ✓	Short: ✗ Long: ✓	✗	✓
d_{N-C}	(✓)	(✓)	(✓)	⊖
E_a	(⊕)	(⊕)	⊖	⊕
$q_{adsorbate}$	✓	(✓)	(⊖)	(✓)
$\mu_{adsorbate}$	(⊕)	(✓)	⊖	(⊖)

Notation: ✓ good, (✓) OK, ✗ wrong, ⊖ too small, (⊖) little too small, ⊕ too large, and (⊕) little too large.

properties.[32–34] As this tube has been cut "straight," this suggests that if the tube is long enough, the details of the cutting scheme are not decisive anymore.

Similarities and discrepancies between both methods are summarized in Table 3. The deviations in local dipoles imply that not even qualitative conclusions can be drawn from the truncated approach, for example, it would suggest that for NH_3, the dipole moment is larger on the metallic CNT than on the semi-conducting one. Under PB conditions, both are equal. Thus, local properties should be evaluated as carefully as adsorption structures. In line with earlier findings, the PB data suggest that chemical gating can be caused by two contributions, dipole and charge transfer effects, for NO_2, and by dipole effects only for NH_3. The sensitivity of NO_2 adsorption to the electronic structure of the nanotube further suggests that this molecule may be prone to chemisorbing (for example at defect sites), whereas NH_3 would be expected to generally physisorb.

Conclusions

To summarize, we have described the supramolecular interactions between metallic and semi-conducting CNTs and NH_3 and NO_2 adsorbates using two different commonly used density functional theory approaches, namely a PB code based on plane-wave single-particle basis functions and pseudopotentials, and a truncated approach based on a localized basis set, where the CNTs were cut and capped by hydrogen atoms. As discussed in the literature, interactions between adsorbates and nanotubes require a careful choice of structural models and computational parameters, in particular proper truncation of CNTs in line with Clar sextet theory,[56] the size of the unit cell potentially leading to interactions between adsorbates in adjacent unit cells,[32,34] the lack of periodicity in truncated structures requiring large structures, the use of pseudopotentials versus all-electron calculations, and the choice of self-consistent field and structure optimization convergence criteria. Ensuring that all these parameters are chosen optimally at the same time is often not possible in practice, in particular when large adsorbates are considered and/or when different adsorption positions or molecular dynamics are relevant. Thus, we focus here on two "reasonable" approaches, which would also be expected to work for large adsorbates, and investigate by comparing them the robustness of different properties with respect to changing computational parameters. We find that cutting semiconducting CNTs according to Clar sextet theory is important for obtaining good adsorption structures, while these structures appear robust with respect to the other parameters. The only exception are flat potential energy surfaces in the binding region (seen here for NH_3), which makes the optimized structures sensitive to the convergence criteria. Adsorption energies and local properties may or may not be described well by truncated approaches—here, a careful selection of computational parameters is more important than for (supra-)molecular structures. The fact that a "straight" truncated (and capped) tube built from three repeating unit cells (and thus featuring three adsorbates) gives very good agreement in terms of local properties with the results obtained under PB conditions, while "Clar" truncated structures (which do not take into account interactions between adsorbates in adjacent unit cells) differ. This suggests that these interactions between periodic images play an important role for the electronic (but not structural) properties, which is in line with previous results from the literature.[32–34] Thus, not only for adsorption energies but also for local properties further research is needed to generate a reliable yet feasible computational protocol for describing molecular adsorbates on CNTs.

Acknowledgment

We thank the University of Hamburg High Performance Computing Centre (RRZ) and the North-German Supercomputing Alliance (HLRN) for computational resources.

Keywords: carbon nanotubes · local properties · density functional theory · noncovalent functionalization

How to cite this article: L. Groß, M. Philipp Bahlke, T. Steenbock, C. Klinke, C. Herrmann. *J. Comput. Chem.* **2017**, *38*, 861–868. DOI: 10.1002/jcc.24760

Additional Supporting Information may be found in the online version of this article.

[1] M. S. Dresselhaus, G. Dresselhaus, P. Avouris, Eds. *Carbon Nanotubes: Synthesis, Structure, Properties and Applications;* Springer Berlin Heidelberg: Germany, **2001**. ISBN http://id.crossref.org/isbn/978-3-540-41086-7.
[2] R. Waser, *Nanoelectronics and Information Technology: Materials, Processes, Devices*, 2nd ed.; Wiley-VCH Verlag GmbH & Co. KGaA: Weinheim, **2005**.
[3] J. Chung, K. H. Lee, J. Lee, D. Troya, G. C. Schatz, *Nanotechnology* **2004**, *15*, 1596.
[4] P. Avouris, Z. Chen, V. Perebeinos, *Nat. Nanotechnol.* **2007**, *2*, 605.
[5] B. F. Habenicht, O. V. Prezhdo, *Nat. Nanotechnol.* **2008**, *3*, 190.
[6] V. Jelicic, M. Magno, K. Chikkadi, C. Roman, C. Hierold, V. Bilas, L. Benini, In *2015 6th IEEE International Workshop on Advances in Sensors and Interfaces (IWASI)*, Gallipoli, Italy, **2015**; pp. 271–276.
[7] A. Hirsch, *Angew. Chem. Int. Ed.* **2002**, *41*, 1853.
[8] E. Y. Li, N. Poilvert, N. Marzari, *ACS Nano* **2011**, *5*, 4455.
[9] Y. S. Lee, N. Marzari, *Phys. Rev. Lett.* **2006**, *97*, 116801.

[10] J. Kong, N. R. Franklin, C. Zhou, M. G. Chapline, S. Peng, K. Cho, H. Dai, *Science* **2000**, *287*, 622.
[11] P. G. Collins, *Science* **2000**, *287*, 1801.
[12] J. Kong, H. Dai, *J. Phys. Chem. B* **2001**, *105*, 2890.
[13] V. Derycke, R. Martel, J. Appenzeller, P. Avouris, *Appl. Phys. Lett.* **2002**, *80*, 2773.
[14] S. Heinze, J. Tersoff, R. Martel, V. Derycke, J. Appenzeller, P. Avouris, *Phys. Rev. Lett.* **2002**, *89*, 106801.
[15] S. Peng, K. Cho, P. Qi, H. Dai, *Chem. Phys. Lett.* **2004**, *387*, 271.
[16] J. Zhang, A. Boyd, A. Tselev, M. Paranjape, P. Barbara, *Appl. Phys. Lett.* **2006**, *88*, 123112.
[17] A. Maiti, J. Hoekstra, J. Andzelm, N. Govind, A. Ricca, A. Svizhenko, H. Mehrez, M. P. Anantram, *NSTI-Nanotechnol.* **2005**, *3*, 236.
[18] A. Sadrzadeh, A. A. Farajian, B. I. Yakobson, *Appl. Phys. Lett.* **2008**, *92*, 022103.
[19] N. Peng, Q. Zhang, C. L. Chow, O. K. Tan, N. Marzari, *Nano Lett.* **2009**, *9*, 1626.
[20] K. Chikkadi, M. Muoth, C. Roman, M. Haluska, C. Hierold, *Beilstein J. Nanotechnol.* **2014**, *5*, 2179.
[21] Y. Li, M. Hodak, W. Lu, J. Bernholc, *Carbon* **2016**, *101*, 177.
[22] A. Goldoni, R. Larciprete, L. Petaccia, S. Lizzit, *J. Am. Chem. Soc.* **2003**, *125*, 11329.
[23] A. Goldoni, L. Petaccia, L. Gregoratti, B. Kaulich, A. Barinov, S. Lizzit, A. Laurita, L. Sangaletti, R. Larciprete, *Carbon* **2004**, *42*, 2099.
[24] A. Goldoni, L. Petaccia, S. Lizzit, R. Larciprete, *J. Phys.: Condens. Matter* **2010**, *22*, 013001.
[25] H. Chang, J. D. Lee, S. M. Lee, Y. H. Lee, *Appl. Phys. Lett.* **2001**, *79*, 3863.
[26] S. Peng, K. Cho, *Nanotechnology* **2000**, *11*, 57.
[27] J. Zhao, A. Buldum, J. Han, J. P. Lu, *Nanotechnology* **2002**, *13*, 195.
[28] S. Peng, K. Cho, *Nano Lett.* **2003**, *3*, 513.
[29] K. Imani, M. R. Abolhassani, A. A. Sabouri Dodaran, *Eur. Phys. J. B* **2010**, *74*, 135.
[30] E. Akbari, Z. Buntat, M. Ahmad, A. Enzevaee, R. Yousof, S. Iqbal, M. Ahmadi, M. Sidik, H. Karimi, *Sensors* **2014**, *14*, 5502.
[31] W. Koch, M. C. Holthausen, *A Chemist's Guide to Density Functional Theory*, 2nd ed.; Wiley VCH: Weinheim, **2001**.
[32] N. Li, G. Lee, J. W. Yang, H. Kim, M. S. Yeom, R. H. Scheicher, J. S. Kim, K. S. Kim, *J. Phys. Chem. C* **2013**, *117*, 4309.
[33] G. Makov, M. C. Payne, *Phys. Rev. B* **1995**, *51*, 4014.
[34] A. Lugo-Solis, I. Vasiliev, *Phys. Rev. B* **2007**, *76*, 235431.
[35] G. N. Simm, M. Reiher, *J. Chem. Theory Comput*. **2016**, 12, 2762–2773.
[36] J. Hutter, M. Iannuzzi, F. Schiffmann, J. VandeVondele, *WIREs Comput. Mol. Sci.* **2014**, *4*, 15.
[37] G. T. Velde, E. J. Baerends, *Phys. Rev. B* **1991**, *44*, 7888.
[38] M. J. Frisch, G. W. Trucks, H. B. Schlegel, G. E. Scuseria, M. A. Robb, J. R. Cheeseman, G. Scalmani, V. Barone, G. A. Petersson, H. Nakatsuji, X. Li, M. Caricato, A. Marenich, J. Bloino, B. G. Janesko, R. Gomperts, B. Mennucci, H. P. Hratchian, J. V. Ortiz, A. F. Izmaylov, J. L. Sonnenberg, D. Williams-Young, F. Ding, F. Lipparini, F. Egidi, J. Goings, B. Peng, A. Petrone, T. Henderson, D. Ranasinghe, V. G. Zakrzewski, J. Gao, N. Rega, G. Zheng, W. Liang, M. Hada, M. Ehara, K. Toyota, R. Fukuda, J. Hasegawa, M. Ishida, T. Nakajima, Y. Honda, O. Kitao, H. Nakai, T. Vreven, K. Throssell, J. A. Montgomery, Jr., J. E. Peralta, F. Ogliaro, M. Bearpark, J. J. Heyd, E. Brothers, K. N. Kudin, V. N. Staroverov, T. Keith, R. Kobayashi, J. Normand, K. Raghavachari, A. Rendell, J. C. Burant, S. S. Iyengar, J. Tomasi, M. Cossi, J. M. Millam, M. Klene, C. Adamo, R. Cammi, J. W. Ochterski, R. L. Martin, K. Morokuma, O. Farkas, J. B. Foresman, D. J. Fox, *Gaussian 09 Revision A.1*; Gaussian, Inc.: Wallingford, CT, **2009**.
[39] P. Giannozzi, S. Baroni, N. Bonini, M. Calandra, R. Car, C. Cavazzoni, D. Ceresoli, G. L. Chiarotti, M. Cococcioni, I. Dabo, A. Dal Corso, S. Fabris, G. Fratesi, S. de Gironcoli, R. Gebauer, U. Gerstmann, C. Gougoussis, A. Kokalj, M. Lazzeri, L. Martin-Samos, N. Marzari, F. Mauri, R. Mazzarello, S. Paolini, A. Pasquarello, L. Paulatto, C. Sbraccia, S. Scandolo, G. Sclauzero, A. P. Seitsonen, A. Smogunov, P. Umari, R. M. Wentzcovitch, et al. *J. Phys.:Condens. Matter* **2009**, *21*, 395502.
[40] D. Corso, *Quantum Espresso Pseudopotentials - PSLibrary 0.3.1*; sISSA: Italy. Available at: http://theossrv1.epfl.ch/Main/Pseudopotentials. Accessed 19 December 2016.
[41] S. Grimme, *J. Comput. Chem.* **2006**, *27*, 1787.
[42] *TURBOMOLE V6.5 2013, a development of University of Karlsruhe and Forschungszentrum Karlsruhe GmbH, 1989-2007, TURBOMOLE GmbH, since 2007. Available at* http://www.turbomole.com.
[43] J. Perdew, K. Burke, M. Ernzerhof, *Phys. Rev. Lett.* **1996**, *77*, 3865.
[44] J. Perdew, K. Burke, M. Ernzerhof, *Phys. Rev. Lett.* **1997**, *78*, 1396.
[45] J. Perdew, K. Burke, Y. Wang, *Phys. Rev. B* **1996**, *54*, 16533.
[46] A. Schäfer, C. Huber, R. Ahlrichs, *J. Chem. Phys.* **1994**, *100*, 5829.
[47] A. D. Becke, *Phys. Rev. A* **1988**, *38*, 3098.
[48] J. P. Perdew, *Phys. Rev. B* **1986**, *33*, 8822.
[49] A. D. Becke, *J. Chem. Phys.* **1993**, *98*, 1372.
[50] C. Lee, W. Yang, R. G. Parr, *Phys. Rev. B* **1988**, *37*, 785.
[51] S. Grimme, J. Antony, S. Ehrlich, H. Krieg, *J, Chem. Phys.* **2010**, *132*, 154104.
[52] S. Grimme, S. Ehrlich, L. Goerigk, *J. Comput. Chem.* **2011**, *32*, 1456.
[53] M. D. Hanwell, D. E. Curtis, D. C. Lonie, T. Vandermeersch, E. Zurek, G. R. Hutchison, *J. Cheminf.* **2012**, *4*, 17.
[54] W. L. Delano, *The PyMOL Molecular Graphics System*; deLano Scientific: Palo Alto, CA, **2002**. Available at: http://www.pymol.org. Accessed 20 September 2016.
[55] G. Schaftenaar, J. Noordik, *J. Comput.-Aided Mol. Des.* **2000**, *14*, 123.
[56] M. Baldoni, A. Sgamellotti, F. Mercuri, *Org. Lett.* **2007**, *9*, 4267.
[57] F. Hirshfeld, *Theor. Chim. Acta* **1977**, *44*, 129.
[58] R. F. W. Bader, P. M. Beddall, *J. Chem. Phys.* **1972**, *56*, 3320.
[59] R. F. W. Bader, P. M. Beddall, *J. Am. Chem. Soc.* **1973**, *95*, 305.
[60] R. F. W. Bader, R. R. Messer, *Can. J. Chem.* **1974**, *52*, 2268.
[61] R. F. W. Bader, P. M. Beddall, J. Peslak, *J. Chem. Phys.* **1973**, *58*, 557.
[62] K. B. Wiberg, P. R. Rablen, *J. Comput. Chem.* **1993**, *14*, 1504.
[63] J. G. Ángyán, G. Jansen, M. Loss, C. Hättig, B. A. Heß, *J. Chem. Phys. Lett.* **1994**, *219*, 267.
[64] R. S. Mulliken, *J. Chem. Phys.* **1955**, *23*, 1833.
[65] P. O. Löwdin, *J. Chem. Phys.* **1950**, *18*, 365.
[66] R. F. W. Bader, C. F. Matta, *Int. J. Quantum Chem.* **2001**, *85*, 592.
[67] K. E. Laidig, R. F. W. Bader, *J. Chem. Phys.* **1990**, *93*, 7213.
[68] R. Bader, T. Keith, K. Gough, K. Laidig, *Mol. Phys.* **1992**, *75*, 1167.
[69] L. Groß, C. Herrmann, *J. Comp. Chem.* **2016**, *37*, 2324.
[70] L. Groß, C. Herrmann, *J. Comp. Chem.* **2016**, *37*, 2260.
[71] G. Henkelman, A. Arnaldsson, H. Jónsson, *Comput. Mater. Sci.* **2006**, *36*, 354.
[72] E. Sanville, S. D. Kenny, R. Smith, G. Henkelman, *J. Comput. Chem.* **2007**, *28*, 899.
[73] W. Tang, E. Sanville, G. Henkelman, *J. Phys.: Condens. Matter* **2009**, *21*, 084204.
[74] D. K. Buck, A. A. Collins, *POV-Ray - The Persistence of Vision Raytracer*. Available at: http://www.povray.org/.
[75] G. Ruiz-Soria, A. Pérez Paz, M. Sauer, D. J. Mowbray, P. Lacovig, M. Dalmiglio, S. Lizzit, K. Yanagi, A. Rubio, A. Goldoni, P. Ayala, T. Pichler, *ACS Nano* **2014**, *8*, 1375.
[76] J. P. Martínez, F. Langa, F. M. Bickelhaupt, S. Osuna, M. Solà, *J. Phys. Chem. C* **2016**, *120*, 1716.
[77] S. Luber, *J. Chem. Phys.* **2014**, *141*, 234110.
[78] S. Luber, M. Iannuzzi, J. Hutter, *J. Chem. Phys.* **2014**, *141*, 094503.
[79] C. R. Jacob, J. Neugebauer, *WIREs Comput. Mol. Sci.* **2014**, *4*, 325.
[80] T. Dresselhaus, J. Neugebauer, *Theor. Chem. Acc.* **2015**, *134*, 97.
[81] K. Azizi, M. Karimpanah, *Appl. Surf. Sci.* **2013**, *285*, 102.

Received: 3 August 2016
Revised: 30 December 2016
Accepted: 9 January 2017
Published online on 28 February 2017